Research Article | Vol. 28, No. 23 / 9 November 2020 / Optics Express 34692
Optics EXPRESS

High-fidelity off-axis digital optical phase conjugation with transmission matrix assisted calibration

CHAITANYA K. MIDIDODDI,[1,3] RACHEL A. LENNON,[1] SHUHUI LI,[1,2] AND DAVID B. PHILLIPS[1,4]

[1] School of Physics and Astronomy, University of Exeter, Stocker Road, Exeter EX4 4QL, UK
[2] Wuhan National Laboratory for Optoelectronics, School of Optical and Electronic Information, Huazhong University of Science and Technology, Wuhan 430074, Hubei, China
[3] c.mididoddi@exeter.ac.uk
[4] d.phillips@exeter.ac.uk

Abstract: The spatial information carried by light is scrambled when it propagates through a scattering medium, such as frosted glass, biological tissue, turbulent air, or multimode optical fibres. Digital optical phase conjugation (DOPC) is a technique that 'pre-aberrates' an illuminating wavefront to compensate for scatterer induced distortion. DOPC systems act as phase-conjugate mirrors: they require a camera to holographically record a distorted wavefront emanating from the scatterer and a spatial light modulator (SLM) to synthesize a phase conjugate of the measured wavefront, which is sent back through the scatterer thus creating a time-reversed copy of the original optical field. High-fidelity DOPC can be technically challenging to achieve as it typically requires pixel-perfect alignment between the camera and SLM. Here we describe a DOPC system in which the normally stringent alignment criteria are relaxed. In our system the SLM and camera are placed in-line in the same optical path from the sample, and the SLM is used in an off-axis configuration. This means high-precision alignment can be achieved by measurement of the transmission matrix (TM) mapping optical fields from the SLM to the camera and vice-versa, irrespective of their relative position. The TM also absorbs and removes other aberrations in the optical system, such as the curvature of the SLM and camera chips. Using our system we demonstrate high-fidelity focussing of light through two ground glass diffusers with a peak-intensity to mean-background ratio of ~700. We provide a step-by-step guide detailing how to align this system and discuss the trade-offs with alternative configurations. We also describe how our setup can be used as a 'single-pixel camera' based DOPC system, offering potential for DOPC at wavelengths in which cameras are not available or are prohibitively expensive.

1. Introduction

Overcoming optical distortion is key to a range of emerging imaging and communication technologies. For example, high-resolution optical imaging of structures deep within biological tissue is a long sought after goal. However, the scattering nature of biological samples partially or fully scrambles the spatial information that is vital for image formation. The spatial modes of light also represent independent information carrying channels that can be used to expand the capacity of optical communication systems. However, harnessing this degree of freedom requires adaptive correction of dynamic aberrations introduced by turbulence in free-space optical communication systems, or mode scrambling in optical fibre-based links. Recently, significant progress has been made in the field of light control, making it possible to mitigate even severe scattering-induced optical distortion [1–5]. The emergence of wavefront shaping techniques have enabled compensation of a medium's linear scattering properties using methods which can be

#409226 https://doi.org/10.1364/OE.409226
Journal © 2020 Received 2 Sep 2020; revised 11 Oct 2020; accepted 12 Oct 2020; published 2 Nov 2020

Optics EXPRESS

broadly categorised into three related approaches: transmission matrix measurement [6], iterative wavefront optimisation [7,8], and optical phase conjugation [9,10].

The transmission matrix (TM) captures the transformation that light fields undergo due to propagation through an opaque object. The TM is a complex-valued linear matrix operator relating the optical field $\mathbf{a}$ incident on a plane at one side of the scatterer, to a transformed field $\mathbf{b}$ exiting at a second plane on another side of the scatterer: $\mathbf{b} = \mathbf{T}_\mathrm{f}\mathbf{a}$. Here $\mathbf{a}$ and $\mathbf{b}$ are complex valued column vectors representing the vectorised 2D light fields on the incident and output planes respectively, and we denote $\mathbf{T}_\mathrm{f}$ as the forward TM from the input to the output plane. $\mathbf{T}_\mathrm{f}$ is measured by sequentially transmitting a set of fields through the sample and recording how each is transformed. Each of these measurements constitutes a single column of the TM (where the TM is represented in a basis governed by the input and output bases). Once obtained, the TM can be used to calculate how to shape light incident on the input plane $\mathbf{a}$, so that it is transformed into a desired target field $\mathbf{b}$ at the output plane: i.e. if $\mathbf{a}$ is set to $\mathbf{a} = \mathbf{T}_\mathrm{f}^{-1}\mathbf{b}$, then the output field is given by $\mathbf{T}_\mathrm{f}\mathbf{a} = \mathbf{T}_\mathrm{f}\mathbf{T}_\mathrm{f}^{-1}\mathbf{b} = \mathbf{b}$ as required [6]. We note that in practice it is sometimes only possible to measure a subset of the TM, which may not be unitary. In this case its inverse can be approximated with the conjugate transpose or computed with the (sometimes regularised) effective- or pseudo-inverse. Therefore the generated output field will approximate the desired output field. Iterative wave-front optimisation is a closely related technique that involves finding the required input $\mathbf{a}$ by repeatedly modulating the input wavefront to improve a figure of merit provided by a feedback signal, such as the intensity of light focussed to a particular point in the sample [7,8].

Optical phase conjugation, also known as 'time-reversal', enables a specified target field to be created after only a single measurement on the scatterer [10]. In this approach, the 'recording' step consists of backwards-propagating the desired target field $\mathbf{d}$ from the output plane to the input plane, and measuring the distorted field $\mathbf{c} = \mathbf{T}_\mathrm{b}\mathbf{d}$ holographically. Here $\mathbf{T}_\mathrm{b}$ is the backward TM through the sample, which is equal to the transpose of the forward TM: $\mathbf{T}_\mathrm{b} = \mathbf{T}_\mathrm{f}^{+}$. Digital optical phase conjugation (DOPC) uses a camera, that is simultaneously illuminated with a coherent reference beam, to measure the distorted field $\mathbf{c}$ [11,12]. In the subsequent 'playback' step, the phase conjugate of the measured field $\mathbf{c}^*$ is then synthesized at the input plane, which forward-propagates through the scattering system, yielding a target field: $\mathbf{T}_\mathrm{b}^{+}\mathbf{c}^* = \mathbf{T}_\mathrm{b}^{+}(\mathbf{T}_\mathrm{b}\mathbf{d})^* = (\mathbf{T}_\mathrm{b}^{\dagger}\mathbf{T}_\mathrm{b}\mathbf{d})^* = \mathbf{d}^*$, i.e. since the synthesized field is the time-reverse of the recorded field, it transforms into the phase conjugate of the target field, $\mathbf{d}^*$, at the output of the scatterer. We note that in general it is only possible to measure a portion of the distorted field, within some solid angle. In this case, analogously with partial TM measurement mentioned earlier, the time-reversed field will approximate the desired output field. Here $(.)^{+}$ and $(.)^{\dagger}$ represent the transpose and conjugate transpose respectively, and in this example the TM is assumed to be unitary so that $\mathbf{T}_\mathrm{b}^{-1} = \mathbf{T}_\mathrm{b}^{\dagger}$. As $\mathbf{T}_\mathrm{b}$ is never measured, then DOPC only requires a single calibration measurement. This means recording and playback can be repeatedly performed on millisecond timescales, enabling focussing through dynamically changing media, such as biological tissue [13], atmospheric turbulence [14] or multimode optical fibres [12]. Using a 'guide-star', coupled with optical memory effects [15–17], DOPC is also suitable for focussing and imaging *inside* scattering materials, where optical access to the target plane is not possible [18–20].

Achieving high-fidelity DOPC is experimentally demanding as it typically requires *pixel-perfect* alignment between the camera used to record the calibration field, and the spatial light modulator (SLM) used to synthesize the time-reversed playback field. Alignment is necessary in six dimensions: translations in 3 dimensions (x, y, z), and tip (θ_x), tilt (θ_y), and rotation (θ_z). Curvature of the camera and SLM screens, along with any other optical aberrations, must also be measured and compensated. Despite these alignment challenges, very high-fidelity DOPC has

Optics EXPRESS

been successfully demonstrated, relying on a variety of bespoke calibration protocols to align such systems [21–24].

In this work, we investigate how the alignment criteria to achieve high-fidelity DOPC may be relaxed. We assess the performance of a DOPC system in which the SLM and camera are placed in-line in the same optical path from the sample, and the SLM is used in an off-axis configuration. This means high-precision alignment can be achieved through measurement of the transmission matrix (TM) mapping optical fields from the SLM to the camera and vice-versa, irrespective of their relative position: minimising the need for physical alignment. As the TM is a completely general operator, it naturally accounts for any translation, rotation and re-scaling between the SLM and camera. In fact there is no longer any need for these elements to be parallel, or in image planes of one another - indeed it is not necessary to precisely know the relative location of the camera and SLM. Here we find it convenient to place the camera approximately in the Fourier plane of the SLM, with a 45° rotation between them. The TM also absorbs the curvature of the SLM and camera chips, and any other aberrations in the optical system. It is still necessary to perform manual alignment between some components - namely single mode fibres and cameras, however the complexity of this remaining task is alleviated as only point-to-point rather than plane-to-plane alignment is required. We provide a guide detailing the steps required to align our setup, discuss trade-offs with respect to other geometries, and demonstrate high-fidelity generation of foci through two ground glass diffusers with an enhancement ratio of ~700.

2. Experimental setup

A schematic of our in-line DOPC system is shown in Fig. 1. The setup is split into two separate optical systems, which here we refer to as the 'switching platform' and the 'DOPC system'. The switching platform and DOPC system are connected through two polarisation maintaining single mode optical fibres: an input and an output fibre. The switching platform enables light from a HeNe laser (Thorlabs HNL150R, wavelength of 633 nm, 15 mW unpolarised) to be transmitted in either direction through the DOPC system, depending upon the position of flip mirrors FM_1 and FM_2. Box 1 shows the flip mirror configuration in the switching platform to send light clockwise, and Box 2 anti-clockwise, through the DOPC system. Figure 2 summarises the main steps in the alignment, calibration and operation of our DOPC system. These steps are described in detail below.

2.1. Alignment and transmission matrix assisted calibration of the optical system

In the absence of a scattering sample, light propagating around the DOPC system in either direction enters via fibre $F_{1/2}$ and is subsequently focussed back into fibre $F_{2/1}$. In order to align the setup we transmit light clockwise without a scattering sample present, which is the case shown in the DOPC schematic in Fig. 1. The path of light entering the DOPC system via F_1 is as follows: Light diverging from fibre F_1 is split by beamsplitter BS_1 into a signal and reference beam. The transmitted signal beam is collimated and the field at the Fourier plane of the input fibre is re-imaged, through an iris I_1, onto the SLM. Our optical system can be implemented with either phase-only SLMs, or binary amplitude SLMs such as digital micro-mirror devices (DMDs). Here we demonstrate the method using a DMD (ViALUX V-7001) of resolution $(s \times t) = (768 \times 1024)$ pixels. The DMD micro-mirrors tilt about their diagonal. We therefore mount the DMD rotated 45° about the optical axis ensuring that the mirror rotation axis is vertical and reflected light remains parallel to the optical bench. The DMD displays a grating pattern to diffract incident light away from the direction of specular reflection. This grating can also incorporate phase variation to correct aberrations in the optical system. Phase correction is required even in the absence of a scatterer, to remove field distortion due to curvature of the DMD screen itself, and any other small aberrations in the system that can reduce the fidelity of the time-reversed field [25]. Light reflecting from the DMD is focussed through a second iris I_2,

Optics EXPRESS

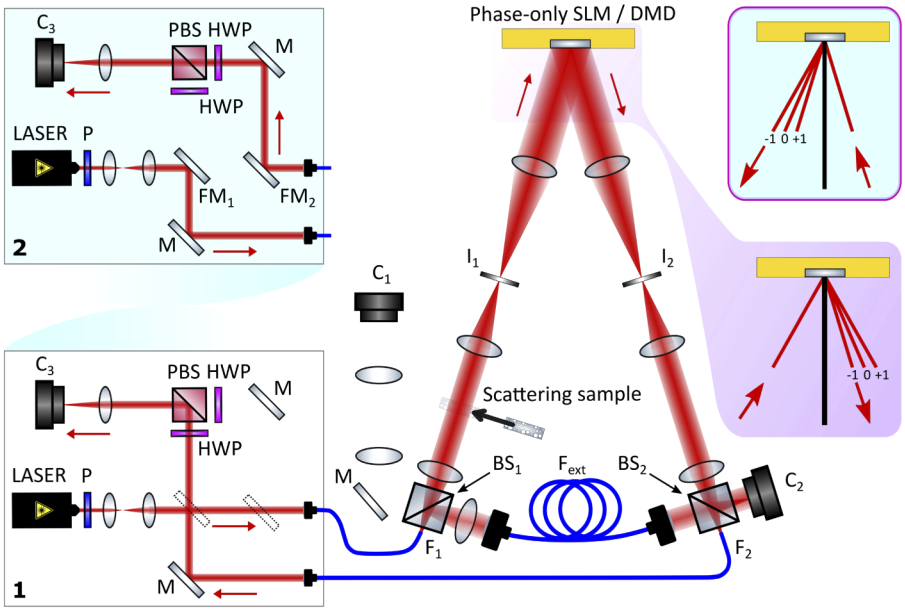

Fig. 1. Experimental setup of the inline DOPC system: C = camera, BS = beamsplitter, P = linear polariser, PBS = polarising beamsplitter, HWP = half wave-plate, M = mirror, FM = flip-mirror, F = polarisation maintaining optical fibre, I = iris (used as a spatial filter). Light emanating from $F_{1/2}$ is collimated by a lens of focal length $f = 60$ mm, and re-imaged onto the DMD with a lens of $f = 150$ mm followed by a lens of $f = 300$ mm. The magnification of the playback field onto camera C_1 is ~ 5. Boxes 1 and 2 show the two possible configurations of the flip mirrors in the switching platform to circulate light clockwise or anti-clockwise around the DOPC system. Light is shown propagating clockwise around the DOPC system, as in the alignment phase. The right-hand insets show which diffraction order is selected by I_1 and I_2 when the light is propagating in either direction.

1. Alignment and Calibration

- Transmit light from fibre F_1, without sample present
- Measure TM $\mathbf{T}$ from DMD to camera C_2
  for $n = 1{:}N$
    Activate super-pixel n
    for $m = 0{:}3$
      Set the phase of active super-pixel to $m\pi/2$
      Record interference pattern on camera C_2
    end
  end
- Display $\boldsymbol{\theta}_{cal}$ on DMD to create a focus at target camera pixel on camera C_2
- Align 3D position of fibre F_2 tip to maximize signal on camera C_3

2. Recording Step

- Insert sample
- Display $\boldsymbol{\phi}_t$ on DMD
- Record distorted field $\mathbf{d}_{cam}$ on camera C_2

3. Playback Step

- Transmit light from fibre F_2
- Display $\boldsymbol{\Psi}_{conj}$ on DMD

Fig. 2. A summary of the main steps in the alignment and calibration of the DOPC system, and the recording and playback phases.

Optics EXPRESS

which passes only the first diffraction order and blocks all other orders. The beam is then split by beamsplitter BS_2, and re-imaged onto both camera C_2 and the tip of single-mode fibre F_2. A coherent reference beam on camera C_2 is formed by light entering the system via fibre F_1 which is reflected by beamsplitter BS_1, then guided by fibre F_{ext} and combined with the signal light at beamsplitter BS_2 to illuminate camera C_2.

The majority of the system alignment is achieved through measurement of the TM that maps how light is transformed from the DMD to camera C_2. The TM is measured using a method similar to that described in [3], by forming an orthogonal set of input modes by sub-dividing the DMD screen into groups of micro-mirrors termed 'super-pixels'. We note that it is also possible to use other input basis representations, such as the Hadamard basis, for example [26]. In this case we choose a super-pixel size of $(p \times q) = (16 \times 16)$ micro-mirrors. A super-pixel is in an active 'on' state when its micro-mirrors are set to display a binary diffraction grating encoding a tilted linear phase function, which across the entire screen is given by $\boldsymbol{\phi}_t \in \mathbb{R}^{s\times t} = k_x\mathbf{x} + k_y\mathbf{y} + \phi_g$ where $\mathbf{x} \in \mathbb{R}^{s\times t}$ and $\mathbf{y} \in \mathbb{R}^{s\times t}$ are 2D arrays, each element of which specifies the Cartesian x- or y-coordinate of the corresponding micro-mirror location on the DMD chip. k_x and k_y specify the x- and y-components of the tilted wave-vector of light diffracted from the DMD, and ϕ_g is a global phase shift.

A binary diffraction grating $\mathcal{B} \in \mathbb{R}^{s\times t}$ encoding an arbitrary bandwidth limited phase function $\boldsymbol{\rho} \in \mathbb{R}^{s\times t}$ on the DMD is given simply by binarising the required phase profile:

$$\mathcal{B} = \frac{1}{2}\text{sgn}[\text{mod}\,(\boldsymbol{\rho}, 2\pi) - \pi] + \frac{1}{2}, \tag{1}$$

where $\text{sgn}[a]$ returns the sign of a. Therefore in this case $\boldsymbol{\rho} = \boldsymbol{\phi}_t$ at coordinates within the bounds of an active super-pixel on the DMD, and 0 otherwise. The diffraction grating within an active super-pixel transmits some of the light from within the super-pixel into the first diffraction order where it passes through iris I_2. A super-pixel is in an 'off' state when all micro-mirrors are set to the same state, and so no light is transmitted into the first diffraction order, and all of the light emanating from this region is blocked by iris I_2.

A sequence of $N = 3072$ orthogonal input modes are used to measure the TM by raster scanning a single active super-pixel over a grid of $(u \times v) = (48 \times 64)$ (determined by super-pixel size) non-overlapping regions across the DMD, while all other super-pixels are turned off. At each super-pixel location, the interference pattern created by light from the active super-pixel interfering with the external reference is recorded in a region of interest on camera C_2 consisting of $M = 61 \times 61 = 3721$ pixels in this case. The phase of this field is recovered using phase stepping holography, by recording the intensity pattern as the global phase of the super-pixel grating is stepped through $\phi_g = 0, \frac{\pi}{2}, \pi, \frac{3\pi}{2}$ rads. Each camera pixel undergoes a sinusoidal variation in intensity as the phase is stepped. The relative phase of these sinusoids encodes the phase of the incident field. The amplitude of the field can also be computed from this data, or directly measured by blocking the reference beam and taking the square-root of the measured intensity. Phase drift between the coherent reference and signal beam can disrupt the TM measurement. To compensate for phase drift, we interlace a field measurement on a standard mode (a single chosen super-pixel) throughout the TM measurement. We track changes to the global phase of this standard measurement which captures the phase drift and enables it to be subtracted from all measurements.

To construct the TM $\mathbf{T} \in \mathbb{C}^{M\times N}$, the field recorded on camera C_2 when the n^{th} input super-pixel is active is vectorised (i.e reshaped into a column vector) and allocated to the n^{th} column of $\mathbf{T}$. $\mathbf{T}$ links an input basis of N super-pixels, to an output basis of M pixels on the camera. As the camera is placed in the Fourier plane of the DMD, then we expect $\mathbf{T}$ to be close to a Fourier Transform matrix. However, $\mathbf{T}$ also encapsulates curvature of both the DMD and camera sensor (if any), the relative scaling of pixels on the two devices, and their relative three dimensional position and orientation, along with other aberrations present in the optical system.

Optics EXPRESS

Once $\mathbf{T}$ is measured we use it to align three image planes: that of the tip of fibre F_1, to the tip of fibre F_2, and both of these to a target camera C_2 pixel of our choosing. To do this we find the calibration phase function $\boldsymbol{\theta}_{\text{cal}}$ that should be encoded into the diffraction grating displayed on the DMD to simultaneously steer a focus to our selected pixel on camera C_2 and remove optical aberrations from the system:

$$\boldsymbol{\theta}_{\text{cal}} = \boldsymbol{\phi}_{\text{t}} + \boldsymbol{\eta}, \tag{2}$$

$$\boldsymbol{\eta} = \arg(\text{reshape}[\mathbf{T}^{\dagger}\mathbf{y}_{\text{pix}}, u, v] \otimes \mathbf{A}). \tag{3}$$

Here $\boldsymbol{\phi}_t$ is the linear phase tilt present inside each super-pixel during TM measurement, and $\boldsymbol{\eta} \in \mathbb{R}^{s\times t}$ is the phase correction to remove DMD curvature and other aberrations, sampled at the resolution of the super-pixels and upscaled via nearest-neighbour interpolation to match the DMD resolution. $\mathbf{y}_{\text{pix}} \in \mathbb{C}^M$ is a column vector of zeros, with a single entry set to one at the position of the element corresponding to the target camera pixel. Therefore $\mathbf{T}^{\dagger}\mathbf{y}_{\text{pix}}$ is the field required on the DMD plane to focus to the target pixel, represented in the super-pixel basis. Here we have set $\mathbf{T}^{-1} = \mathbf{T}^{\dagger}$, under the assumption that $\mathbf{T}$ is unitary as there are minimal losses in the system. The operator reshape$[\mathbf{x}, u, v]$ reshapes a column vector $\mathbf{x} \in \mathbb{C}^N$ to a $u \times v$ element array, representing the dimensions of the super-pixels on the DMD. $\mathbf{A}$ is a $p \times q$ matrix of ones, and the kronecker product $\otimes$ serves to upscale the reshaped super-pixel representation to the full $s \times t$ resolution of the DMD. Figure 3(a) shows an example of phase function $\boldsymbol{\eta}$ for our system - depicting the non-flat nature of the DMD screen.

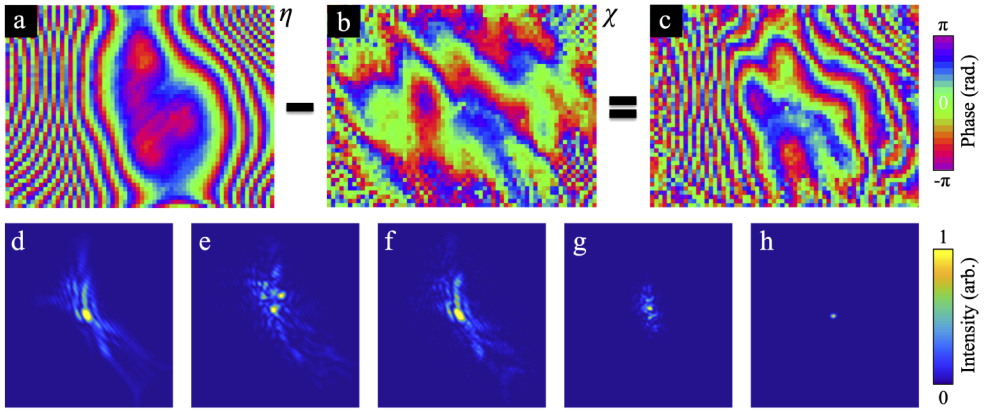

Fig. 3. Weak phase aberration: (a) shows the phase correction required for the DMD itself ($\boldsymbol{\eta}$). (b) shows the phase correction required for the sample ($\boldsymbol{\chi}$). (c) shows the combined phase correction. (d) shows the intensity of the distorted focus in the absence of the sample, without DMD curvature correction. (e) shows further distortion to the focus when the weak phase aberration is placed in the setup. (f) shows the focus with the implementation of sample aberration correction, but without DMD curvature correction. (g) shows the focus with the implementation of DMD curvature correction without sample aberration correction. (h) shows the intensity of the time-reversed field when both DMD curvature correction and sample aberration correction are applied on the DMD. Each panel (d-h) has a linear scale and is normalised to its own peak intensity. The peak intensity increases by a factor of ~8 from (g) to (h).

$\boldsymbol{\theta}_{\text{cal}}$ is encoded into a binary diffraction pattern to display on the DMD using Eq. (1) with $\boldsymbol{\rho} = \boldsymbol{\theta}_{\text{cal}}$. When displayed, light emanating from F_1 passes through the DOPC system and focusses to our target pixel on C_2. A focus is simultaneously also created in the vicinity of the tip of fibre F_2. To overlap the tip of fibre F_2 with this focus, the 3D position of the tip of fibre F_2 is manually adjusted to maximise the total intensity of return light measured at camera C_3 on the

Optics EXPRESS

switching platform. We note that as only the total intensity is required then C_3 could also be replaced with a photo-diode. When this intensity is maximised then the images of the tips of fibres F_1 and F_2, and our selected camera C_2 pixel, are all aligned, and any native aberrations in the optical system have been removed. Light can now pass in either direction through the DOPC system, and the alignment phase is complete.

2.2. Recording step

The scattering sample is inserted into the beam path as shown in Fig. 1. The sample can be placed at any point in between beam-splitter BS_1 and Iris I_1. To record the distortion of the target field due to the sample, light transmitted from fibre F_1 passes through the sample and propagates clockwise around the DOPC system. The linear phase tilt function $\boldsymbol{\phi}_t$ is encoded into the diffraction grating displayed on the DMD with all super-pixels active. The first diffraction order passes through I_2 and is imaged by camera C_2, where it interferes with the external reference beam. The distorted optical field arriving at camera C_2, given in vectorised form by $\mathbf{d}_{\text{cam}} \in \mathbb{C}^M$, is measured in four camera frames using phase stepping holography by changing the global phase of the DMD grating as before. We note that the field on C_2 could also be measured in a single camera frame using digital holography, by sacrificing the spatial resolution of the measurement by a factor of two in each dimension.

2.3. Playback step

Once the distorted field emanating from the sample is measured, the direction of propagation of light around the DOPC system is reversed by switching the position of flip mirrors FM_1 and FM_2 (as shown in Box 2 in Fig. 1), and so light is emitted from fibre F_2. The external reference beam path is now blocked. We use the TM to transform the measured distorted field at the camera plane, $\mathbf{d}_{\text{cam}}$, to the *synthesis plane* - this is the plane that light passes through immediately *after* diffracting from the DMD (when propagating anti-clockwise from fibre F_2) - and the plane at which we will synthesise the desired phase conjugate field. The measured field at the synthesis plane is given by $\mathbf{d}_{\text{synth}} \in \mathbb{C}^N = \mathbf{T}^\dagger \mathbf{d}_{\text{cam}}$, here represented in the super-pixel basis. Therefore, the playback phase function encoded into the DMD diffraction grating to synthesize a time-reversed field to transmit back through the sample is given by:

$$\boldsymbol{\psi}_{\text{conj}} = \boldsymbol{\theta}_{\text{cal}} - \boldsymbol{\chi}, \tag{4}$$

$$\boldsymbol{\chi} = \arg(\text{reshape}[\mathbf{d}_{\text{synth}}, u, v] \otimes \mathbf{A}). \tag{5}$$

Here $\boldsymbol{\chi}$ is the time-reversed argument of $\mathbf{d}_{\text{synth}}$, that has been reshaped and up-scaled - i.e. this is the phase function we aim to generate at the phase-conjugate synthesis plane. $\boldsymbol{\theta}_{\text{cal}}$, previously calculated in Eq. (2), is also necessary in Eq. (4) to remove the DMD induced aberration in the *playback* beam transmitted from fibre F_2 to the synthesis plane. As before, $\boldsymbol{\psi}_{\text{conj}}$ is encoded into the binary diffraction pattern displayed on the DMD using Eq. (1) where $\boldsymbol{\rho} = \boldsymbol{\psi}_{\text{conj}}$. Camera C_1 is used to image the time-reversed field once it has passed back through the sample.

3. Results

We first test the performance of our in-line DOPC system by using it to time-reverse the field that has propagated through a weakly aberrating media: a thin phase screen, formed from three pieces of stressed plastic sandwiched together, the phase of which vary slowly with position. This sample was placed 2 cm from the image plane of the DMD. Figure 3(b) shows $\boldsymbol{\chi}$, the measured phase aberration induced by the weak scatterer. Figure 3(c) shows the resulting phase pattern that should be encoded into the tilted diffraction grating displayed on the DMD to time-reverse the distorted field. Figures 3(d)-(h) show the images of the intensity of the playback field back-propagated through the sample, captured by C_1 under different conditions, highlighting the

Optics EXPRESS

effect of the different terms in Eq. (4). Figure 3(d) shows the distorted focus in the absence of the sample, without DMD curvature correction, i.e. in this case the DMD encodes only the linear phase ramp: $\boldsymbol{\rho} = \boldsymbol{\phi}_t$ to direct incident light into the first diffraction order. Figure 3(e) shows further distortion to the focus when the sample is placed in the setup. Figure 3(f) shows the focus with the implementation of sample aberration correction, but without DMD curvature correction, i.e. $\boldsymbol{\rho} = \boldsymbol{\phi}_t - \boldsymbol{\chi}$. This looks similar to Fig. 3(d) as we would expect. Figure 3(g) shows the focus with the implementation of DMD curvature correction without sample aberration correction: $\boldsymbol{\rho} = \boldsymbol{\theta}_{cal}$, isolating only the sample induced distortion. Finally, Fig. 3(h) shows the intensity of the time-reversed field when both DMD curvature correction and sample aberration correction are applied on the DMD: $\boldsymbol{\rho} = \boldsymbol{\psi}_{conj}$, yielding diffraction limited focussing, and increasing the peak intensity of the focus by a factor of ~8 in comparison with Fig. 3(g).

Next, we test the performance of our in-line DOPC system when tasked with focussing through a more severe aberration: two ground glass diffusers (220 grit and 1500 grit polish) placed near the image plane of the DMD. We chose to focus through two diffusers to ensure we test a multiple scattering scenario. Figures 4(a) and (b) show $\mathbf{d}_{cam}$ and $\mathbf{d}_{synth}$ respectively. Figure 4(c) shows the phase pattern $\boldsymbol{\psi}_{conj}$ encoded into the DMD diffraction grating to time-reverse the distorted field. Figure 4(d) shows the diffraction limited spot at camera C_1 when the full phase correction shown in Fig. 4(c) is applied. Figure 4(e) shows the intensity at camera C_1 prior to phase correction: the diffusers fragment the beam into a speckle pattern. Figure 4(h) shows a comparison of line-profiles through the intensity patterns on C_1 with and without phase correction.

To quantify the fidelity of the focussing, we calculate the enhancement factor Σ, given by the ratio between the peak intensity of the time-reversed focus, and the average intensity of the residual background speckle pattern. When focussing through the sample formed from two diffusers, we find $\Sigma \sim 700$. This figure can be compared to the theoretically expected enhancement factor for phase only modulation: $\Sigma_t \sim \frac{\pi}{4} N_{eff}$, where N_{eff} is the number of orthogonal spatial modes (in our case super-pixels) controlled on the SLM [1]. The theoretical enhancement factor is derived under the assumption that (i) the phase correction applied to each super-pixel is statistically independent, and that (ii) each super-pixel contributes equally to the total intensity. Therefore, should these assumptions be satisfied in our system (i.e. $N_{eff} = N = 3072$), we would expect an enhancement factor of $\Sigma_t \sim 2400$. However, in our case, the intensity of the playback field is a Gaussian beam chosen to fit inside, rather than overfill, the DMD chip, as shown in the inset in Fig. 4(h). Therefore, super-pixels towards the edge of the DMD contribute significantly less power to the focus than those in the middle of the DMD and our experiment does not comply with assumption (ii) in the estimation of the theoretical enhancement factor given above.

In our proof-of-principle experiment, approximately half of the super-pixels control the majority of the power in the playback field, and so we estimate that $N_{eff} \sim 1500$, and so the theoretically expected Σ_t is reduced by a factor of ~ 2 to $\Sigma_t \sim 1200$. Our experimentally obtained enhancement factor increases to $\Sigma \sim 1000 \sim 0.8\Sigma_t$ when focussing through a single diffuser (220 grit polish), positioned at the image plane of the DMD. In this case, we attribute the observed increase in Σ to the fact that the single diffuser acts as a pure phase screen and the intensity of the recorded field is well matched to the playback field intensity at the DMD (i.e. they are both Gaussian beams of similar beam waist). Meanwhile, when focussing through two diffusers, the intensity profile of the distorted beam is broadened at the DMD plane, thus overspilling the area of the playback beam. Therefore we conclude that the main factor reducing the enhancement factor from that theoretically predicted when focussing through a multiple scattering sample is the narrow beam waist of the Gaussian intensity profile of the playback field. This could be readily improved by expanding the playback beam to overfill the SLM chip. Other factors that contribute to a reduction in Σ may include: any correlations in the distorted field between adjacent super-pixels, which further reduce the effective number of independently controllable modes N_{eff}; small errors in the measurement of the complex elements of the TM; small errors

Optics EXPRESS

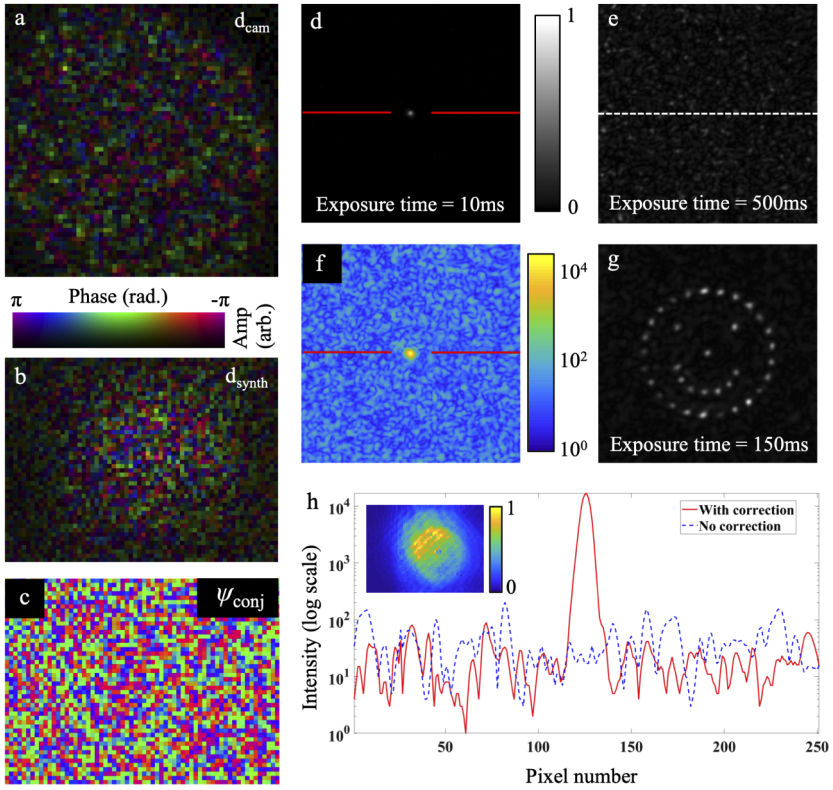

Fig. 4. Strong phase aberration, focussing light through two ground glass diffusers: (a) the field measured on the camera: $\mathbf{d}_{\text{cam}}$. (b) the calculated field at the DMD plane: $\mathbf{d}_{\text{synth}}$. (c) the phase correction encoded into the DMD (note: there is also a linear phase gradient $\boldsymbol{\phi}_{\text{t}}$ encoded into each super-pixel, which is not shown). (d) the resulting focus imaged on camera C_1, which can be compared with (e) the speckle when no correction is applied. (f) The same data as (d) now displayed on a log-plot: created by combining data from multiple exposures. (g) Focussing 35 spots through the diffuser simultaneously using the tilt-memory effect. (d,e,h) have a linear greyscale scale bar. (h) Line-profiles through the generated focus (red solid line, also marked on (d) and (f)), and through the uncorrected speckle (blue dashed line, also marked on (e)). Enhancement factor $\Sigma \sim 700$ in this case. The inset in (h) shows an estimate of the intensity profile I of the playback beam on the DMD. This is given by $I = \left|\text{reshape}[\mathbf{T}^{\dagger}\mathbf{y}_{\text{pix}}, u, v]\right|^2$ which is the measured intensity of each super-pixel as light propagates around the system from F_1 without a sample present. As the system is symmetric we expect this to have a similar intensity profile to the playback field propagating from F_2.

Optics EXPRESS

associated with the approximation that $\mathbf{T}^{-1} = \mathbf{T}^{\dagger}$; and any drift in the alignment of the optical system in between calibration and playback. Nonetheless, the levels of enhancement we achieve with our system are comparable with the focussing achievable with TM-based approaches using a similar number of super-pixels, in which measured and corrected fields are transmitted in the same direction and so are automatically aligned [25].

Ground glass diffusers exhibit an angular memory effect: tilting of the incident wavefront results in a corresponding tilt in the wavefront emerging from the output side of the diffuser, thus causing a lateral shift in the optical field in the far-field of the output [15,17]. This effect arises as a consequence of the strongly diagonal nature of the real-space transmission matrix of the diffuser itself [27]. Figure 4(g) shows the generation of an array of focussed spots on C_1 using the angular memory effect. In this experiment a single diffuser (220 grit polish) was placed in the Fourier plane of camera C_1, which corresponds to the image plane of the DMD. Due to the angular memory effect, the time-reversed field focussed onto C_1 can be translated simply by adding an additional phase tilt to the phase correction pattern encoded onto the DMD. To create an array of $K = 35$ foci simultaneously, we encode $\boldsymbol{\psi}_{\text{array}}$ onto the DMD, where:

$$\boldsymbol{\psi}_{\text{array}} = \arg\left[\sum_{k=1}^{K} \exp\left(i\left(\boldsymbol{\psi}_{\text{conj}} + \delta k_x^k \mathbf{x} + \delta k_y^k \mathbf{y}\right)\right)\right]. \tag{6}$$

Here k indexes the spot number, and δk_x^k and δk_y^k specify the tilts in x and y to translate the k^{th} focussed spot on C_1. As the diffuser can be considered a single phase screen, then in this case the angular memory effect range of the diffuser is much greater than the area into which we project the array of foci [28]. In Fig. 4(g) the mean enhancement factor of the foci is $\Sigma \sim 30$. The main reason for the reduction in contrast when multiple foci are generated, in comparison with the single focus case, is because the intensity has now been split over multiple spots, while the intensity of the speckled background has remained approximately the same level (i.e. $\frac{\Sigma_{\text{SingleFocus}}}{K} = \frac{1000}{35} \sim 30$).

Figure 4(g) also shows some variation in the intensity of the spots in the foci array. There are two contributing factors that give rise to this non-uniformity. Firstly, phase only modulation means the field required to create a uniform spot array is not precisely created (i.e. it has the wrong amplitude profile). The created DOPC field has a varying level of correlation with the fields required to create each individual focus. This results in a variation in the efficiency with which each focussed point is generated. This phenomenon occurs whenever phase-only control is used to create spot arrays - even without focussing the array through a scattering medium. A number of algorithms have been developed (primarily for use in holographic optical tweezers experiments) to equalise the intensities of the spots [29]. Secondly, the non-uniformity of the spot array is exacerbated by the uncontrolled light scattered into the background speckle pattern: this speckle interferes constructively with some spots, enhancing the intensity at those locations, but interferes destructively with others, reducing the intensity of those foci.

4. Discussion and conclusions

In this article we have described a DOPC system in which the SLM and camera are placed in-line in the same optical path from the sample, and the SLM is used in an off-axis configuration. This means high-precision alignment can be achieved through measurement of the TM mapping optical fields from the SLM to the camera and vice-versa, irrespective of their relative position and orientation. The TM accounts for any re-scaling between the pixels of the devices, and also absorbs and removes other aberrations in the optical system such as the curvature of the SLM and camera chips. We have shown that our DOPC system performs well when tasked with focussing light through a multiple scattering sample formed by two ground glass diffusers. We now discuss

Optics EXPRESS

some of the trade-offs in this system compared to other DOPC configurations, and some potential avenues for development.

Our in-line configuration is compatible with both phase-only SLMs, and binary amplitude SLMs such as the DMD demonstrated in this work. If a phase-only SLM is employed, the phase conjugating function $\boldsymbol{\psi}_{\text{conj}}$ can be directly applied. In the case of a DMD, $\boldsymbol{\psi}_{\text{conj}}$ is encoded into a binary amplitude function through Eq. (1) as described above. DMDs offer the advantage of fast modulation, however we note that their use as diffractive optics should only be considered in situations with high signal levels, as the binary amplitude grating introduces considerable losses of ~95% both during the recording and playback steps. In contrast, diffractive use of phase-only SLMs suffer a more moderate loss of ~20-40% [25].

Light propagating in either direction around the set up passes through a spatial filter after diffracting from the SLM (irises I_1 and I_2). These spatial filters are necessary to select only the first diffraction order, ensuring both the measured and playback fields are captured/replayed with high-fidelity. We note that the spatial filters only block light at spatial frequencies that we are unable to generate in the playback field using the super-pixel approach, and so there is no intrinsic loss associated with them within the spatial band limit of our system. The disadvantage of this approach is that by using the SLM to steer light into the first diffractive order, the highest spatial frequency in the recorded/playback fields is limited to a resolution lower than the full SLM resolution.

In our present configuration the spatial resolution of the phase conjugated field, which is given by the resolution of the super-pixels, is a factor of 16 times lower in each dimension than the resolution of the DMD itself. We note that it is possible to further decrease the size of the super-pixels to increase the playback field resolution. For example, Ref. [25] previously demonstrated DMD-based TM measurements with a super-pixel size of $(p \times q) = (4 \times 4)$ micro-mirrors, which in our case would increase the resolution to $N = 49152$ super-pixels. Nonetheless, our super-pixel based DOPC approach does sacrifice resolution, and so the trade-off is as follows: our method enables high bit-depth phase control, and so the creation of high-fidelity, yet lower-resolution playback fields; versus, for example, previous DMD-based DOPC systems which use the DMD at its full resolution, but are limited to lower bit-depth binary amplitude [13] or binary phase control (in the latter case by employing a phase contrast configuration [30]), and so generate lower-fidelity playback fields. Therefore our system is particularly well-suited to high-fidelity time-reversal of fields of moderate spatial bandwidth, such as found in free-space optical communication systems [14], or multi-mode optical fibres [12,31].

In this work we have used the SLM to control only the phase of each super-pixel in the playback field, however, our approach is also compatible with (lossy) amplitude modulation: tuning the efficiency of each playback super-pixel by diffracting some of the light striking a super-pixel to other diffraction orders where it is blocked by the spatial filter [32,33]. Using this approach, it would also be straightforward to extend our setup to perform vectorial time-reversal, by measuring and structuring fields in two orthogonal polarisation states simultaneously [34]. This could be achieved with high stability via a single phase-only SLM or DMD using, for example, the methods detailed in Refs. [35–37].

The time taken for calibration of our system is also worth consideration. Here we measure the TM by scanning through $N = 3072$ super-pixels with the DMD synchronised with camera C_2 at a rate of 100 Hz. Therefore the TM calibration phase takes ~3 minutes (excluding DMD loading time). This time includes 5 measurements per super-pixel (4 phase steps and an intensity measurement with the external reference beam blocked). However, we note there is scope to significantly decrease this calibration time to a few seconds: it was recently shown that with a little prior knowledge of what to expect, TM measurement can be achieved from a drastically reduced measurement set by employing the framework of compressed sensing [38,39]. In the case of our DOPC system there is potential to leverage knowledge of the approximate relative

Optics EXPRESS

positions of the DMD and camera as priors (and the fact that the TM is expected to be close to a Fourier transform) to recover the full TM from only a few measurements.

Finally, we highlight that our setup can also be operated in a 'single-pixel complex-field camera' mode, requiring only a point intensity measurement and removing the need for a camera in the alignment and recording steps. In this case, alignment can be achieved by using an alternative reference beam provided by activating a second static 'reference' super-pixel on the SLM in addition to the active 'signal' super-pixel that is raster-scanned over the SLM. Light from the two active super-pixels interferes at the tip of fibre F_2, which forms the 'single-pixel' of the single-pixel camera. The intensity illuminating the tip of fibre F_2 can be measured by camera C_3 (which could also be replaced by a photo-diode). As the phase of the signal super-pixel is modulated, the intensity at the tip of fibre F_2 fluctuates, enabling calculation of the phase of light emanating from the signal super-pixel relative to the reference to be calculated [3]. By raster-scanning the signal super-pixel over the SLM, we can reconstruct the relative phase of all super-pixels required to constructively interfere at the location of the tip of fibre F_2. This is equivalent to measurement of $\boldsymbol{\theta}_{\text{cal}}$. The same process can be followed with the sample in place, enabling measurement of the distorted wavefront and thus calculation of $\boldsymbol{\chi}$. We tested this single-pixel camera-based DOPC approach, and found equivalent performance to the camera-based method. The main disadvantage of this single-pixel method is that measurement of each back-propagated distorted wavefront requires $4N$ sequential measurements, and so it is a factor of N slower than recording a full-field measurement with a camera when the signal-to-noise ratio is held constant (although we note that the use of a high-speed photodiode could mean that the measurement rate may be limited by the modulator - such as 20 kHz rate DMD - rather than the detector). The key advantage of the single-pixel approach is that it avoids the need for a camera, and so it could enable DOPC at wavelengths where cameras do not yet exist, or are prohibitively expensive [40,41].

Funding

Royal Academy of Engineering; European Research Council (804626).

Acknowledgments

DBP thanks the Royal Academy of Engineering and the European Research Council for financial support.

Disclosures

The authors declare no conflicts of interest.

Data Availability

The raw data for this paper is available at http://hdl.handle.net/10871/123251.

References

1. I. M. Vellekoop and A. Mosk, "Focusing coherent light through opaque strongly scattering media," Opt. Lett. **32**(16), 2309–2311 (2007).
2. I. M. Vellekoop and A. Mosk, "Universal optimal transmission of light through disordered materials," Phys. Rev. Lett. **101**(12), 120601 (2008).
3. T. Čižmár, M. Mazilu, and K. Dholakia, "In situ wavefront correction and its application to micromanipulation," Nat. Photonics **4**(6), 388–394 (2010).
4. A. P. Mosk, A. Lagendijk, G. Lerosey, and M. Fink, "Controlling waves in space and time for imaging and focusing in complex media," Nat. Photonics **6**(5), 283–292 (2012).
5. S. Rotter and S. Gigan, "Light fields in complex media: Mesoscopic scattering meets wave control," Rev. Mod. Phys. **89**(1), 015005 (2017).

Optics EXPRESS

6. S. Popoff, G. Lerosey, R. Carminati, M. Fink, A. Boccara, and S. Gigan, "Measuring the transmission matrix in optics: an approach to the study and control of light propagation in disordered media," Phys. Rev. Lett. **104**(10), 100601 (2010).
7. I. M. Vellekoop and A. Mosk, "Phase control algorithms for focusing light through turbid media," Opt. Commun. **281**(11), 3071–3080 (2008).
8. D. B. Conkey, A. N. Brown, A. M. Caravaca-Aguirre, and R. Piestun, "Genetic algorithm optimization for focusing through turbid media in noisy environments," Opt. Express **20**(5), 4840–4849 (2012).
9. G. S. He, "Optical phase conjugation: principles, techniques, and applications," Prog. Quantum Electron. **26**(3), 131–191 (2002).
10. Z. Yaqoob, D. Psaltis, M. S. Feld, and C. Yang, "Optical phase conjugation for turbidity suppression in biological samples," Nat. Photonics **2**(2), 110–115 (2008).
11. M. Cui and C. Yang, "Implementation of a digital optical phase conjugation system and its application to study the robustness of turbidity suppression by phase conjugation," Opt. Express **18**(4), 3444–3455 (2010).
12. I. N. Papadopoulos, S. Farahi, C. Moser, and D. Psaltis, "Focusing and scanning light through a multimode optical fiber using digital phase conjugation," Opt. Express **20**(10), 10583–10590 (2012).
13. D. Wang, E. H. Zhou, J. Brake, H. Ruan, M. Jang, and C. Yang, "Focusing through dynamic tissue with millisecond digital optical phase conjugation," Optica **2**(8), 728–735 (2015).
14. Y. Zhou, J. Zhao, B. Braverman, K. Pang, R. Zhang, A. E. Willner, Z. Shi, and R. W. Boyd, "Turbulence suppression using phase conjugation for mode-division multiplexing over a 340-m free-space link," arXiv preprint arXiv:2010.00128 (2020).
15. J. Bertolotti, E. G. Van Putten, C. Blum, A. Lagendijk, W. L. Vos, and A. P. Mosk, "Non-invasive imaging through opaque scattering layers," Nature **491**(7423), 232–234 (2012).
16. H. Yılmaz, C. W. Hsu, A. Goetschy, S. Bittner, S. Rotter, A. Yamilov, and H. Cao, "Angular memory effect of transmission eigenchannels," Phys. Rev. Lett. **123**(20), 203901 (2019).
17. S. Li, S. A. Horsley, T. Tyc, T. Cizmar, and D. B. Phillips, "Guide-star assisted imaging through multimode optical fibres," arXiv preprint arXiv:2005.06445 (2020).
18. X. Xu, H. Liu, and L. V. Wang, "Time-reversed ultrasonically encoded optical focusing into scattering media," Nat. Photonics **5**(3), 154–157 (2011).
19. Y. Liu, C. Ma, Y. Shen, J. Shi, and L. V. Wang, "Focusing light inside dynamic scattering media with millisecond digital optical phase conjugation," Optica **4**(2), 280–288 (2017).
20. R. Horstmeyer, H. Ruan, and C. Yang, "Guidestar-assisted wavefront-shaping methods for focusing light into biological tissue," Nat. Photonics **9**(9), 563–571 (2015).
21. M. Jang, H. Ruan, H. Zhou, B. Judkewitz, and C. Yang, "Method for auto-alignment of digital optical phase conjugation systems based on digital propagation," Opt. Express **22**(12), 14054–14071 (2014).
22. M. Azimipour, F. Atry, and R. Pashaie, "Calibration of digital optical phase conjugation setups based on orthonormal rectangular polynomials," Appl. Opt. **55**(11), 2873–2880 (2016).
23. H. Ruan, J. Brake, J. E. Robinson, Y. Liu, M. Jang, C. Xiao, C. Zhou, V. Gradinaru, and C. Yang, "Deep tissue optical focusing and optogenetic modulation with time-reversed ultrasonically encoded light," Sci. Adv. **3**(12), eaao5520 (2017).
24. A. S. Hemphill, Y. Shen, J. Hwang, and L. V. Wang, "High-speed alignment optimization of digital optical phase conjugation systems based on autocovariance analysis in conjunction with orthonormal rectangular polynomials," J. Biomed. Opt. **24**(03), 1 (2018).
25. S. Turtaev, I. T. Leite, K. J. Mitchell, M. J. Padgett, D. B. Phillips, and T. Čižmár, "Comparison of nematic liquid-crystal and dmd based spatial light modulation in complex photonics," Opt. Express **25**(24), 29874–29884 (2017).
26. D. B. Conkey, A. M. Caravaca-Aguirre, and R. Piestun, "High-speed scattering medium characterization with application to focusing light through turbid media," Opt. Express **20**(2), 1733–1740 (2012).
27. B. Judkewitz, R. Horstmeyer, I. M. Vellekoop, I. N. Papadopoulos, and C. Yang, "Translation correlations in anisotropically scattering media," Nat. Phys. **11**(8), 684–689 (2015).
28. N. Antipa, G. Kuo, R. Heckel, B. Mildenhall, E. Bostan, R. Ng, and L. Waller, "Diffusercam: lensless single-exposure 3d imaging," Optica **5**(1), 1–9 (2018).
29. R. Di Leonardo, F. Ianni, and G. Ruocco, "Computer generation of optimal holograms for optical trap arrays," Opt. Express **15**(4), 1913–1922 (2007).
30. C. Ma, F. Zhou, Y. Liu, and L. V. Wang, "Single-exposure optical focusing inside scattering media using binarized time-reversed adapted perturbation," Optica **2**(10), 869–876 (2015).
31. Y. Zhou, B. Braverman, A. Fyffe, R. Zhang, J. Zhao, A. E. Willner, Z. Shi, and R. W. Boyd, "High-fidelity spatial mode transmission through multimode fiber via vectorial time reversal," arXiv preprint arXiv:2003.09883 (2020).
32. W.-H. Lee, "Binary computer-generated holograms," Appl. Opt. **18**(21), 3661–3669 (1979).
33. J. A. Davis, D. M. Cottrell, J. Campos, M. J. Yzuel, and I. Moreno, "Encoding amplitude information onto phase-only filters," Appl. Opt. **38**(23), 5004–5013 (1999).
34. Y. Shen, Y. Liu, C. Ma, and L. V. Wang, "Focusing light through scattering media by full-polarization digital optical phase conjugation," Opt. Lett. **41**(6), 1130–1133 (2016).

Optics EXPRESS

35. C. Maurer, A. Jesacher, S. Fürhapter, S. Bernet, and M. Ritsch-Marte, "Tailoring of arbitrary optical vector beams," New J. Phys. **9**(3), 78 (2007).
36. T. Čižmár and K. Dholakia, "Exploiting multimode waveguides for pure fibre-based imaging," Nat. Commun. **3**(1), 1027 (2012).
37. K. J. Mitchell, S. Turtaev, M. J. Padgett, T. Čižmár, and D. B. Phillips, "High-speed spatial control of the intensity, phase and polarisation of vector beams using a digital micro-mirror device," Opt. Express **24**(25), 29269–29282 (2016).
38. E. J. Candès and M. B. Wakin, "An introduction to compressive sampling," IEEE Signal Process. Mag. **25**(2), 21–30 (2008).
39. S. Li, C. Saunders, D. J. Lum, J. Murray-Bruce, V. K. Goyal, T. Cizmar, and D. B. Phillips, "Compressively sampling the optical transmission matrix of a multimode fibre," arXiv preprint arXiv:2007.15891 (2020).
40. P. Sen, B. Chen, G. Garg, S. R. Marschner, M. Horowitz, M. Levoy, and H. P. Lensch, "Dual photography," in *ACM SIGGRAPH 2005 Papers*, (2005), pp. 745–755.
41. M. P. Edgar, G. M. Gibson, and M. J. Padgett, "Principles and prospects for single-pixel imaging," Nat. Photonics **13**(1), 13–20 (2019).